Numerical study of geometrical effects on the performance of an H-type cylindrical resonant photoacoustic cell [†]

Madhusoodanan Mannoor[1], Jeeseong Hwang[2] and Sangmo Kang[1,*]

[1]*Department of Mechanical Engineering, Dong-A University, Busan 49315, Korea*
[2]*Applied Physics Division, National Institute of Standards and Technology, Boulder, CO 80305, USA*

Abstract

We have numerically studied the geometrical effects on the performance of an H-type cylindrical resonant photoacoustic cell, composed of one resonator and two symmetrical buffer cylinders, by performing simulations on the generation of acoustic waves in the cell. Here, the acoustic response (pressure), resonance frequency and quality factor are calculated for the cell performance, while the lengths and diameters of both resonator and buffer cylinders are considered for the geometrical parameters or dimensions. Our calculation solves linearized forms of the continuity equation, Navier-Stokes equation, energy equation, and equation of state using a finite element method under an assumption that the heat addition due to the laser passage and thus the variations in the velocity, pressure and temperature fields inside the cell are small enough. First, we performed a statistical analysis using a design of experiment method to evaluate the relative impacts of the cell dimensions on the acoustic response. Subsequently, we performed a parametric study to quantify the cell performance with the dimensional variations. Our results, along with the response surface methodology, provide guidance for a systematic design optimization of the cell for the best acoustic response. The approach in this study may be applied to the design of various types of resonant photoacoustic spectroscopy devices.

Keywords: H-type cell; Optimization; Photoacoustic pressure; Quality factor; Resonant photoacoustic cells

---

1. Introduction

The generation of sound when a material is irradiated with non-stationary light, a well-known photoacoustic phenomenon, was first reported by Bell [1, 2] in his path- breaking papers "On the production and reproduction of sound by light" and "The production of sound by radiant energy", published in 1880 and 1881, respectively. A molecule in a material, upon absorption of photon, gets excited and if it does not lose this excess energy other than by collision with other molecules, the net kinetic energy of the molecules increases, thereby increasing the temperature of the material. If the excitation by light is periodic, the temperature rise in the material is also periodic, leading to alternating expansion and contraction of the material to trigger sound waves. This phenomenon can be used to develop various kinds of sensors for environmental, biological and medical applications [3-6].

The photoacoustic spectroscopy, because of its non-destructive nature and versatility, has a wide range of applicability in various materials, ranging from soft tissues to liquids and gases. It is recognized as an effective and inexpensive method to investigate and characterize the properties of a matter. Since the absorption of photons is needed for the generation of a photoacoustic signal, the scattered or transmitted radiation does not affect the photoacoustic response. This feature is excellent for trace gas analysis, where the number of absorbing molecules is very small. Thus, a variety of photoacoustic sensors developed based on these characteristics have shown excellent sensitivity on the level of a part per trillion (ppt) [7]. Since the amount of energy absorbed by the gas is miniscule, the acoustic response is also very weak. However, the constructive interference contributed by the boundary at acoustic resonance may be used to achieve high acoustic response amplitudes (pressure) which are detectable by a microphone. The resonant frequencies corresponding to various modes of longitudinal or radial resonance in the case of a cylindrical photoacoustic cell can be calculated by analytical methods. If the frequency of the light source is the same as the natural frequency corresponding to a particular mode of the photoacoustic cell, the resonance can be achieved. Such a resonant photoacoustic cell has widely been used for various spectroscopic applications [7, 8].

The ability to generate high amplitudes of acoustic pressure at a microphone for a given amount of absorbed radiation is one of the most pertinent design objectives for resonant

---

*Corresponding author. Tel.: +82 51 200 7636, Fax.: +82 51 200 7656
   E-mail address: kangsm@dau.ac.kr

photoacoustic cells. The sensitivity of the photoacoustic cell depends strongly on its geometry. Up to now, different shapes such as H, T and 'banana' have been proposed to enhance the acoustic response [8-11]. In the H-type cell which has a resonator cylinder and two buffer cylinders, the buffer structure strongly affects the acoustic response. Selection of the dimensions of the buffer cylinders becomes a significant part of the design of an H-type photoacoustic cell. As the laser beam passes through windows of the photoacoustic cell, some quantity of light energy may be absorbed by the windows, which can generate acoustic waves. Such undesirable waves are known as window noises. Bijnen et al. [3] suggested that the ideal buffer cylinder length should be a quarter of the acoustic wavelength in order to minimize the window noises, whereas the resonance frequency and quality factor are not much affected by the buffer cylinder length. Cai et al. [7] also suggested that the buffer cylinder length should be equal to a quarter of the acoustic wavelength in order to extract the best acoustic signal. However, they reported significant variations in the resonance frequency with the buffer cylinder length.

The acoustic wave motion at a monofrequency is governed by the Helmholtz equation [12]. Since the heat added to the gas by the photoacoustic effect acts as a source for the generation of sound waves, the acoustic waves in a photoacoustic cell can also be described by the Helmholtz equation with a source term corresponding to the photoacoustic generation. In the literature, the governing equations have typically been solved by the method of expansion of eigenmodes [8]. The eigenmode expansion method was introduced to solve the inhomogeneous Helmholtz equation, where the exact eigenmodes can be found by solving the homogenous Helmholtz equation [8]. However, the analytical solution based on the Helmholtz equation is possible only for regular geometries, limiting its utility in real applications. To overcome this limitation, numerical simulations have been performed by coupling the finite element method (FEM) technique with the eigenmode expansion method in order to find the acoustic response in photoacoustic cells of various shapes [9, 10]. Here, the thermal and viscous losses in the cells can be well accounted for by including the quality factor in the calculation of the acoustic pressure. Most of the studies on modelling of resonant photoacoustic cells developed for spectroscopic applications, reported in the last decade, are based on this method [9, 10, 13, 14]. However, when the eigenmode expansion method, in which the acoustic pressure field alone is determined by superimposing the eigenmodes, is applied to model the acoustic response in a photoacoustic cell, the expansion is truncated after the first eight modes to simplify the calculation [9, 10]. Therefore, the error in the eigenmode expansion method is expected to be large. Another drawback of this method is that it is not a direct way of calculating the acoustic pressure. Even if we use a commercial software to calculate the eigenmodes, further calculations are needed, which include the estimation of quality factor, to find out the amplitude of acoustic pressure at the point of interest. Instead of using the eigen-

mode expansion method, an alternative method to solve for all the acoustic variables would be beneficial for the improved simulation of photoacoustic response in a resonant cell.

Compared to the eigenmode expansion method, it would be highly accurate to predict the acoustic response by directly solving the full set of the continuity equation, Navier-Stokes equation, energy equation, and equation of state. By this method, we can develop a model that includes the thermal and viscous losses associated with the wave propagation and solve for all the acoustic variables, which makes it more realistic than the eigenmode expansion method. The aforementioned method has been used by a few researchers to solve various acoustic problems [15-17]. In the present study, we want to extend it to the case of an H-type resonant photoacoustic cell. For accurate and effective estimation of thermal and viscous losses, we adopt a combination of a very fine mesh near the walls, where viscous and thermal boundary layers exist, and a normal mesh in the bulk region, where the thermal and viscous losses are negligible. If such a holistic approach is followed, we will be able to more accurately analyze the effect of geometry on the key design features of a resonant photoacoustic cell than the previously reported numerical studies on the same topic [3, 7]. Apart from the above, considering the range of applications, optimization of the geometrical parameters or dimensions of a resonant photoacoustic cell is an interesting topic of research. The existing literature [3, 7], which touches upon the topic of the optimization of resonant photoacoustic cells, is not based on any standard procedure to follow in the optimization problems. The study reported by Kost et al. [10] deals with the shape optimization of a cell, not with the optimal dimensions of a predefined shape. To the best of our knowledge, however, any statistical study of the geometrical effects on the performance of a cylindrical resonant photoacoustic cell, which would provide the foundation needed to develop a metamodel (or surrogate model) based optimization technique, has not so far been reported. So, if an accurate numerical simulation method, which is much closer to the actual physics, is used as a tool to conduct a statistical analysis, it would save resources needed to carry out an equivalent number of physical experiments. This strongly motivates the present study.

The main objective of the present study is to numerically investigate the geometrical effects on the performance of an H-type cylindrical resonant photoacoustic cell, composed of one resonator and two symmetrical buffer cylinders. Here, the H-type cell is chosen because it is one of the simplest and most widely used designs for gas spectroscopic applications. An FEM-based software was used to perform simulations on the generation of acoustic waves in the cell under an assumption that the heat addition due to the laser passage and thus the variations in the velocity, pressure and temperature fields inside the cell are sufficiently small. For this study, we solve the full set of linearized forms of the continuity equation, Navier-Stokes equation, energy equation and equation of state for the key performance parameters such as the acoustic response,

resonance frequency and quality factor. First, we perform a statistical analysis using a design-of-experiment (DOE) method to see the relative effects of the dimensions of the H-type cell on the acoustic response. Next, we perform a parametric study to further understand the variation of the cell performance in response to the dimensional changes. Lastly, we carry out a design optimization of the cell by employing a response surface methodology (RSM) to explore the possibility of systematically optimizing the resonant photoacoustic cell based on a metamodel or surrogate model.

2. Numerical methods

This section explains the H-type photoacoustic cell considered in this study and then presents the governing equations and numerical methods used to predict the performance of the cell according to the geometrical parameters or dimensions.

2.1 H-type photoacoustic cell

In this study, a numerical analysis was performed on an H-type resonant photoacoustic cell, composed of one cylindrical resonator with a size of $L_r \times D_r$ (length and diameter) and two symmetric buffer cylinders (volumes) with a size of $L_b \times D_b$ attached at both ends of the resonator, as shown in Fig. 1. The cell is assumed to be filled with a gaseous medium, butane, at a temperature of 300 K and a pressure of 100 kPa (1 atm) in an equilibrium state, whose properties used for the simulations are listed in Table 1. The laser beam supplied on the left-hand side passes through the longitudinal axis of the resonator towards right. The photoacoustic response was measured in terms of the acoustic pressure at the position of microphone, located at the center of the resonator.

2.2 Mathematical modelling

The photoacoustic response, characterized by the acoustic pressure at the position of microphone, can be numerically predicted by solving for the pressure field inside the cell, in close relation with the acoustic waves generated by the photoacoustic effect. Assuming the fluid flow (butane gas) to be compressible, viscous and Newtonian, the acoustic waves triggered by the photoacoustic effect are governed by the continuity equation, Navier-Stokes equation, energy equation, and equation of state [17]. In the case of acoustic wave propagation in a gaseous medium, it is assumed that the ranges of variations in the density, velocity, pressure and temperature fields should be much smaller than their respective background values at an equilibrium state. The density, velocity, pressure, and temperature fields, therefore, can be approximately expressed as small harmonic oscillations about their background values. Under such an assumption, each of the variables can be decomposed into an equilibrium part and a fluctuating part in the frequency domain. For example, the velocity $\mathbf{u}$ can be decomposed as $\mathbf{u} = \mathbf{u_0} + \mathbf{u'}e^{i\omega t}$, where the first and second terms represent the equilibrium part and fluctuat-

Table 1. Properties of butane considered in the present study.

Property	Value
Specific heat at constant pressure, C_p	1675 J/(kg K)
Density, ρ	2.376 kg/m³
Ratio of specific heats, γ	1.085
Coefficient of thermal expansion, α	8.750×10^{-4} /K
Speed of sound, c	210.59 m/s
Thermal conductivity, k	0.016 W/(m K)
Dynamic viscosity, μ	7.600×10^{-6} Pa s
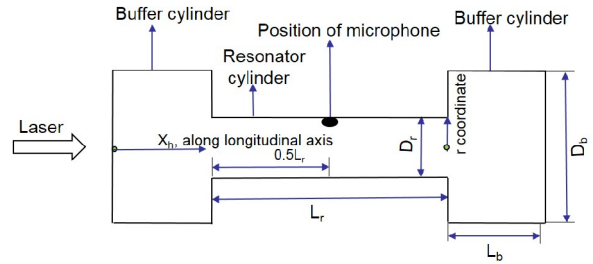
Fig. 1. Schematic diagram of the H-type resonant photoacoustic cell considered in the present study.

ing part, respectively. The final equations after linearization of the basic equations can be written as follows [18]:

$$i\omega\rho' + \rho_0 (\nabla \cdot \mathbf{u'}) = 0, \tag{1}$$

$$i\omega\rho_0 \mathbf{u'} = \nabla \cdot \begin{pmatrix} -p'\mathbf{I} + \mu\left(\nabla\mathbf{u'} + (\nabla\mathbf{u'})^T\right) \\ -\left(\dfrac{2\mu}{3} - \mu_B\right)(\nabla \cdot \mathbf{u'})\mathbf{I} \end{pmatrix}, \tag{2}$$

$$i\omega\rho_0 C_p T' = -\nabla \cdot \left(-k\nabla T'\right) + i\omega p' T_0 \alpha_0 + H', \tag{3}$$

$$\rho' = \rho_0 \left(\beta_T p' - \alpha_0 T'\right). \tag{4}$$

where ρ, p and T are respectively the density, pressure and temperature fields, μ, μ_B, C_p, α, β_T and k denote respectively the dynamic viscosity, bulk viscosity, specific heat at a constant pressure, thermal expansion coefficient, isothermal compressibility, and thermal conductivity, H is the heat source, t is the time, and I is the identity matrix. ω is the angular frequency of the laser beam, given by $2\pi f$ where f is the pulsation frequency (the inverse of the pulse repetition rate) of the laser, and i is the imaginary unit. In addition, the subscript '0' denotes the equilibrium steady state (ρ_0, T_0 and α_0) and the prime (') represents the small fluctuating amplitude of each variable. The heating of the gas by the absorption of laser beam can be modelled using the primed heat source, H'. Assuming the Gaussian profile for the laser beam, the heat source, at a radial position relative to the centerline of the resonator can be approximated as [13]

$$H'(r) = aI_0 \exp\left[-2\left(\frac{r^2}{w^2}\right)\right] \tag{5}$$

where r is the radial coordinate, w is the radius of laser beam, a is the absorption coefficient and I_0 is the power of the laser.

The actual propagation of acoustic waves in a photoacoustic cell is damped by the thermal and viscous losses. When we consider the bulk region of the medium away from the surface, the wave motion can be considered nearly adiabatic and the effect of viscosity is also marginal. Hence, the losses in the bulk region, which are minimal, are termed as volume losses. On the other hand, the losses caused by the thermal conduction and viscous friction near the wall, termed as surface losses, form a significant part of the total losses. To account for the loss mechanism in the photoacoustic cell, generally the concept of quality factor is used. In the eigen-mode expansion method, we need to calculate the quality factor at various eigenmodes to find the amplitude of pressure. In the present study, to the contrary, estimation of the quality factor is not needed at all because we directly solve the governing equations. However, for the purpose of analyzing the effect of geometrical parameters on the loss mechanism of the cell, we calculated the quality factor only at the operating mode 'j' of the cell. The quality factor, Q_j, at the resonance frequency corresponding to the j-th mode is defined as the ratio of the resonance frequency to its full width half maximum (FWHM):

$$Q_j = \frac{f_j}{\Delta f_j} \tag{6}$$

where f_j is the resonance frequency and Δf_j is the FWHM.

Although the requirements of the desired resonant photoacoustic cell are subjective depending on the applications, the high sensitivity, which ensures that the photoacoustic response has a detectable magnitude, is a key requirement in all the cases. The amplitude of the photoacoustic response (pressure) becomes high when the resonance frequency is low. However, the microphone noise would be of considerable magnitude at a low frequency, which makes it necessary to keep the resonance frequency above the widely accepted lower threshold, 1000 Hz. A larger cell volume would increase the quality factor, but a smaller volume is favourable for increasing the amplitude of response. In real applications, an appropriate trade-off between the sensitivity and the other key parameters such as resonance frequency and quality factor would be necessary. For the effective measurement of the acoustic pressure generated from the target gas species, the signal to noise ratio at the position of microphone should be as high as possible. However, an experimental investigation is the most suitable method to properly quantify the noise at the position of microphone. In the present numerical analysis, therefore, the window noise is not considered. Here, we want to focus on three parameters, the acoustic response (pressure), resonance frequency and quality factor, when we analyze the performance of the H-type photoacoustic cell.

2.3 Numerical formulation and validation

The numerical formulation and validation necessary for simulating the photoacoustic response in an H-type resonant photoacoustic cell are discussed in this section. For the study, we numerically solved linearized forms of the governing Eqs. (1)-(4) for the photoacoustic response and resonance frequency using the thermoacoustic interface of the acoustic module of COMSOL Multiphysics software based on an FEM [18]. Here, the resonance was identified as a spike in the frequency response plot, in which the acoustic pressure is plotted against the pulsation frequency of the laser, f [9]. Through the simulations, we can predict the key performance parameters of the cell, such as the acoustic response (pressure), resonance frequency and quality factor, by varying the geometrical parameters, such as lengths and diameters of the resonator and two symmetric buffer cylinders. At the last stage of the present study, we executed a systematic design optimization of the cell by employing an RSM and then found the optimal dimensions for maximizing the acoustic response in order to explore the possibility of application of our method to optimal sizing of the cell.

The photoacoustic response was calculated in terms of the acoustic pressure at the position of microphone. Since the response is actually measured as an amplified microphone signal, an arbitrary value can be assigned for the term, aI_0, in Eq. (5) [13]. Here, we assign $aI_0 = 1$ for all the simulations. A radius of 2 mm was considered for the laser beam in all simulations. At all the boundaries, the isothermal and no-slip conditions were applied. Non-uniform, free tetrahedral elements were chosen for discretizing the domain. In the numerical modelling of the sound waves, a rule of thumb is to have at least five elements per wavelength [13]. In the present study, since we are interested only in the first longitudinal mode of resonance while simulating cells with different sizes, the frequencies range from 1000 Hz to 3000 Hz. A frequency step of 1 Hz was used between two consecutive frequency values. The minimum wave length of acoustic waves in our simulations, which would correspond to the maximum frequency of laser beam, given by (c/3000 Hz), approximately equals to 70 mm. We chose to use a maximum element size of 2 mm so that the minimum number of elements per wavelength is around 35, ensuring a high degree of accuracy. However, the thermoacoustic modelling demands finer mesh to incorporate the heating effect due to the laser beam passing through the longitudinal axis of the resonator. In the laser beam path, the maximum element size was restricted to 1 mm. In order to verify the mesh independence, the mesh sizes in the beam path and in the rest of the cell were restricted to 0.5 mm and 1 mm, respectively, and the effects on the acoustic pressure and resonance frequency were simulated. The variations in the acoustic pressure and resonance frequency were less than 0.8 % of the corresponding values at the previous mesh sizing. Based on the mesh independence test, to optimize the computational time for all simulations, the maximum element size in

the laser beam path and in the rest of the cell were fixed at 1 mm and 2 mm, respectively. In addition, the presence of thermal and viscous boundary layers needs to be taken care at all the boundaries. For the range of frequencies under investigation in the present study, the thickness of boundary layers is between 50 and 250 μm. In the corresponding part of the mesh, the maximum element size was limited to 10 μm.

We validated the numerical method employed in the present study by adopting three different resonance problems whose theoretical, numerical or experimental results are available in literature: The first one is an H-type cell, the second one is a Helmholtz cell and the third is a simple closed cell. Here, we assumed that the cells were filled with nitrogen gas in the first and third problems, whereas it was with air in the second one. In all the three problems, a temperature of 293 K and a pressure of 101 kPa (1 atm) were assumed. The above assumptions were made to match the present conditions with the corresponding ones specified in the experimental or numerical studies available in literature. Kost et al. [10] performed both numerical analysis based on the eigenmode expansion method and experimental study for an H cell and they are taken as the reference for validation in the present study. We performed numerical simulations on the same H-type photoacoustic cell considered in the reference and compared our results with theirs. The resonance frequency corresponding to the first longitudinal mode is found to be 2743 Hz in the present study and the experimental result reported in the reference is 2753 Hz. The relative deviation is just 0.36 %, whereas the corresponding value from the eigenmode expansion based method reported in the above reference is 1.2 %. The frequency responses obtained by the present method in the range of frequencies of 2500 Hz to 3000 Hz, which has equal spread on either side of the first longitudinal resonance frequency, were compared with the corresponding experimental and numerical results reported in the reference. To allow a reasonable comparison between microphone responses obtained from the experiment with pressure responses obtained from the numerical analysis in the reference, both have been normalized with respect to their maximum values. We also followed the same procedure. Fig. 2 shows the comparison between our results and the reference results. The normalized response obtained by the present method is much closer to the experimental result, in comparison with the numerical result obtained by the eigenmode expansion method. So, it can be deduced that the present model estimates the photoacoustic response with better accuracy than the eigenmode expansion based model.

Gliere et al. [16] used similar numerical method employed in the present study to simulate the photoacoustic response in a Helmholtz photoacoustic cell. We also numerically predicted the acoustic pressure in two chambers of the microsized Helmholtz photoacoustic cell described in the above reference and then compared our results with theirs as shown in Fig. 3. Excellent agreement between our results and the previous numerical results confirms the validity of the present
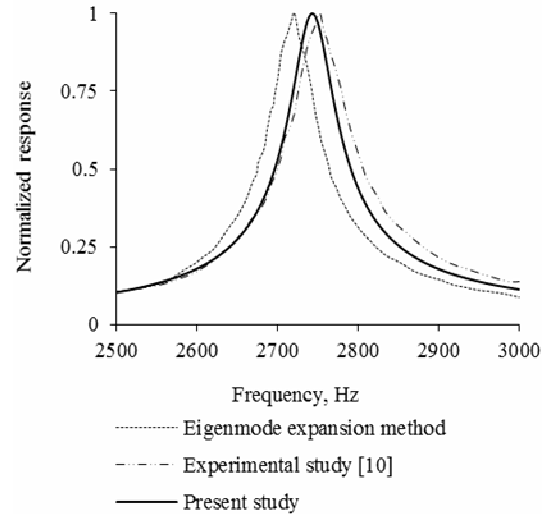
Fig. 2. Validation of the present numerical method for the H-type photoacoustic cell: Frequency response curve obtained in the present study, after normalizing with the peak response, compared with the results of the experimental and numerical studies of Kost et al. [10].
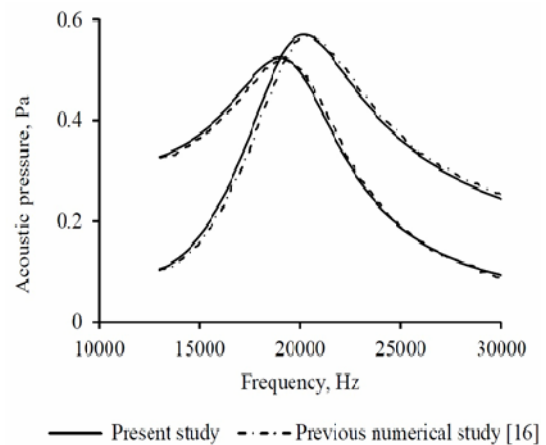
Fig. 3. Validation of the present numerical method for the Helmholtz photoacoustic cell: Frequency response curves in two chambers of the Helmholtz cell obtained in the present study, compared with the results of the numerical study of Gliere et al. [16].

numerical model.

Subsequently, we performed numerical simulations on the acoustic waves in a simple cell, composed of a single cylindrical resonator closed at both ends, and then compared their result with the available analytical solution [9] given as

$$f_{1,\text{anal}} = \frac{c}{2L_r} \tag{7}$$

where f_1 is the natural resonance frequency corresponding to the first longitudinal mode of the cylinder. Fig. 4 shows the variation of the resonance frequency, computed with the present numerical method, with the resonator length. Here, the numerical resonance frequency was obtained by identifying the peak position corresponding to the first longitudinal mode

in the acoustic pressure versus frequency plot for each simulation. In addition, the present result was also compared with the analytical solution in the same figure. The comparison indicates that the present result is in fairly good agreement with the analytical solution with the maximum deviation of around 1.4 %, validating the present numerical method. From the three different validations mentioned above, we concluded that our numerical method and simulations are meaningful enough for the purpose of the present study.

3. Results and discussion

In order to understand the effects of the geometrical parameters on the photoacoustic response of the H-type resonant photoacoustic cell, in this section, we perform numerical simulations on the cell using an FEM based software and then discuss their results.

3.1 Statistical analysis of the H-type cell

We applied the Taguchi method of robust design [19], which is a well-known design of experiment (DOE) method, to the H-type cell and then conducted a series of numerical experiments to statistically analyze the effects of the geometrical parameters on the photoacoustic response. In the DOE method, one variable out of different variables associated with the physical problem is identified as a response parameter, while the other ones, whose values can be controlled so that the response parameter can be either maximized or minimized, are termed as control parameters. In the present study, the acoustic pressure at the position of microphone is the response parameter because we want to maximize it by adjusting the geometrical parameters of the cell. We chose four control parameters: length and diameter of the resonator, L_r and D_r, and length and diameter of both symmetric buffer cylinders, L_b and D_b. In the Taguchi method, to analyze the effects of variations of the control parameters on the response, we need to assign certain values to the control parameters. These values are called levels. Since all the parameters are continuous variables, two levels were adopted for each of these parameters for the initial set of experiments, as suggested by Ross et al. [19].

The initial levels adopted for the control parameters are listed in Table 2. The basic idea in the DOE method is to find out the effects of variations of the control parameters and their interactions on the response with a possible minimum number of experiments. Here, interactions indicate the effects of combined variations of multiple control parameters on the response data. Therefore, we need to intelligently pick combinations of levels of the control parameters for each experiment. The orthogonal array, which is a well-known combinatorial design, is widely used in such problems. In the present study, since we have four control parameters, eleven number of interactions are possible among them. So, an impact analysis of variations of a total number of fifteen control parameters and interactions is discussed here. The data needed for such an

Table 2. Values of the control parameters corresponding to the two levels adopted for the present study.

Level	L_r / mm A	D_r / mm B	L_b/ mm C	D_b/ mm D
1	40	6	20	14
2	80	12	40	28

Table 3. Assignment of the control parameters and their interactions in the L16 array used for the present study.

Column number of L16 array	Control parameter / interaction
1	A
2	B
3	$A \times B$
4	C
5	$A \times C$
6	$B \times C$
7	$A \times B \times C$
8	D
9	$A \times D$
10	$B \times D$
11	$C \times D$
12	$A \times B \times D$
13	$A \times C \times D$
14	$B \times C \times D$
15	$A \times B \times C \times D$
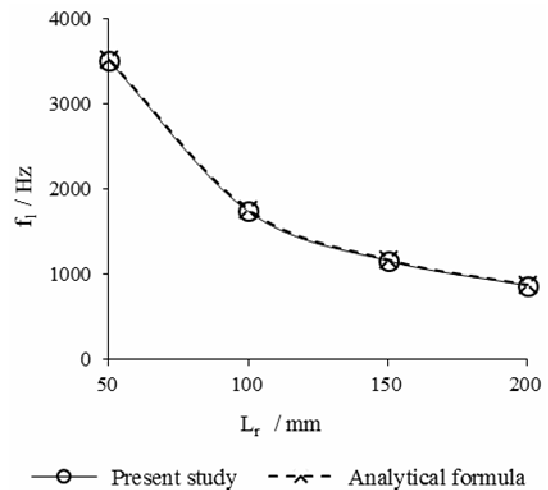
Fig. 4. Validation of the present numerical method for the simple cell: variation of the resonance frequency corresponding to the first longitudinal mode with the resonator length, compared with the analytical solution, Eq. (7).

analysis can be generated by performing simulations with the control parameters at the stipulated levels, as given in an L16 orthogonal array [19]. Table 3 shows the assignment of the control parameters and their mutual interactions in the L16

Table 4. Acoustic pressures measured from the initial experiments for the present study.

Trial number	L_r / mm	D_r / mm	L_b / mm	D_b / mm	Acoustic pressure / mPa
1	40	6	20	14	4.014×10^{-1}
2	40	6	20	28	6.105×10^{-1}
3	40	6	40	14	3.099×10^{-4}
4	40	6	40	28	3.117×10^{-4}
5	40	12	20	14	1.324×10^{-4}
6	40	12	20	28	1.976×10^{-1}
7	40	12	40	14	1.877×10^{-4}
8	40	12	40	28	8.000×10^{-4}
9	80	6	20	14	5.057×10^{-1}
10	80	6	20	28	6.875×10^{-1}
11	80	6	40	14	5.531×10^{-1}
12	80	6	40	28	6.358×10^{-1}
13	80	12	20	14	2.100×10^{-4}
14	80	12	20	28	3.933×10^{-1}
15	80	12	40	14	2.668×10^{-4}
16	80	12	40	28	1.762×10^{-1}

array. Subsequently, we conducted a series of simulations according to the standard L16 array configuration, which are termed as initial experiments in the DOE terminology, and then presented their results in Table 4. Table 4 shows the acoustic pressure at the microphone position measured as a photoacoustic response corresponding to each of different trials in the initial experiments.

Next, we analyzed the effects of the control parameters on the acoustic pressure based on the response data collected from the experiments using the analysis of variance (ANOVA), which forms the crux of the design of experiment philosophy. Various terms used in ANOVA applicable to the present study are briefly explained below. Let the response value for a particular trial be y_i and the total number of experiments be N. The total sum of squares, SS_T, which shows the net variation from a mean value of response considering all the trials in the initial experiments, is calculated by

$$SS_T = \left(\sum_{i=1}^{N} y_i^2\right) - \frac{1}{N}\left(\sum_{i=1}^{N} y_i\right)^2 . \tag{8}$$

The average response, $\overline{X}_k$, for any parameter X corresponding to its level k is the mean of y_i for all the n trials associated with the parameter value, X_k. Therefore, the sum of squares corresponding to a particular parameter, X, denoted by SS_X is given by

$$SS_X = n\left(\sum_{k=1}^{n} \left(\overline{X}_k\right)^2\right) - \frac{1}{N}\left(\sum_{i=1}^{N} y_i\right)^2 . \tag{9}$$

The sum of squares for each particular parameter is the measure of deviation of the response from the mean value, which can be attributed to that parameter. However, if we consider all the parameters and their interactions, some of them may not have a considerable effect on the response. To identify the control parameters and interactions which have significant effects on the response, we used the so-called F test. The sums of squares for all of the control parameters and interactions are compared through the F test to find the significant sources of variations. All the individual sums of squares were arranged in an ascending order and then the second smallest one was divided by the smallest one, which would give the F ratio. The significant F ratio for a control parameter/interaction can be referred from the standard statistical tables [19]. If the F ratio from the first two smallest sums of squares is not significant, then, their sum was calculated and the third smallest sum of square was divided by it. This process continued until we found a significant F ratio. In order to use the standard tables for the F test, we need to know the degree of freedom corresponding to each control parameter/interaction. The degree of freedom, ϕ_X, is given by the number of its levels minus one and the total degree of freedom, ϕ_T, is the total number of trials. When we add individual sums of squares of two control parameters/interactions, their degrees of freedom also get added. Finally, when we found the first significant F ratio, individual sums of squares of all control parameters/interactions, which were considered prior to that, were added together to constitute the error, which represents the portion of total sum of squares, that can be attributed to insignificant control error parameters/interactions. In other words, the sum of squares due to error is given by

$$SS_e = SS_T - \sum SS_X \tag{10}$$

where $\sum SS_X$ represents the sum of sums of squares with significant F ratios for all the parameters and interactions. Therefore, the degree of freedom of the error term is calculated by

$$\phi_e = \phi_T - \sum \phi_X . \tag{11}$$

Then the variance of a control parameter, V_X, is given by

$$V_X = \frac{SS_X}{\phi_X} . \tag{12}$$

The F ratio of a control parameter is given by

$$F_X = \frac{V_X}{V_e} \tag{13}$$

where V_e is the variance of error.

The results obtained from ANOVA performed on the initial experiments are summarized in Table 5. While all four control parameters have significant effects on the response, their in-

Table 5. Results of ANOVA obtained from the initial experiments for the present study.

Parameter	ϕ_x	Sum of Squares, SS	Percentage contribution	F ratio	Confidence level
A	1	1.900×10^{-7}	17.00	7.74	95 %
B	1	4.310×10^{-7}	38.70	17.60	99 %
C	1	1.280×10^{-7}	11.50	5.22	95 %
D	1	9.610×10^{-8}	8.63	3.92	90 %
Error	11	2.700×10^{-7}	-	-	-
Total	15	1.110×10^{-6}	-	-	-

teractions do not cause any significant variation of the response. So, the sum of sums of squares of all the interactions can be clubbed together as the error. The individual sum of squares and percentage contribution toward the total sum of squares for each control parameter, as shown in this table, clearly show that the diameter of the resonator has the most significant effect on the photoacoustic response. From the statistical tables, for each F ratio, the corresponding confidence level is also shown. For example, from the present study, it can be said with 95 % confidence that the length of the resonator is a significant factor which determines the photoacoustic response. Since the sensitivity in a photoacoustic cell is usually inversely proportional to the volume of the cell, selecting the smallest possible diameter of the resonator would yield the highest photoacoustic response. In practice, however, it would not be possible to arbitrarily minimize the resonator diameter. In general, the radius of laser beam used in the photoacoustic cells is around 1.5 mm to 2 mm [5]. Therefore, the radius of resonator needs to be greater than 2 mm, the microphone needs to be placed at the center of the resonator, and the buffer cylinders have to be mechanically assembled with the resonator. Considering these constraints, we decided to fix the resonator diameter at 6 mm. Note that the same value was already used in Gillis et al. [5] to fabricate an experimental setup associated with the H-type cell. To understand the effects of the other control parameters except the resonator diameter, therefore, we continued to perform more simulation by varying L_r, L_b and D_b and then discussed the effects in the next subsection.

3.2 Parametric study on the H-type cell

To understand the geometrical effects on the performance of the H-type cell, we considered three factors: photoacoustic response measured as acoustic pressure at the location of microphone, the quality factor of the cell and the resonance frequency.

In order to understand the geometrical effects on the photoacoustic response, two different sets of simulations were performed. In the first set, L_r and L_b were varied while the diameter of the buffer cylinder is kept constant at D_b = 14 mm. Fig. 5
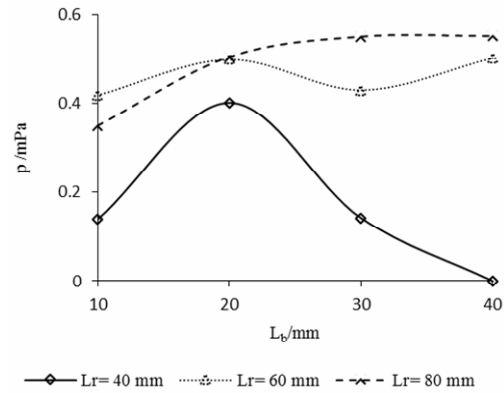
Fig. 5. Variations of the acoustic pressure at the position of microphone with the length of the buffer cylinder at different resonator lengths for the H-type cell. Here, the diameter of the buffer cylinder is kept constant at D_b = 14 mm.

shows the acoustic pressure measured at the location of microphone, plotted against the buffer cylinder length for various lengths of the resonator. Results indicate that the acoustic pressure is significantly influenced by L_r and L_b. It is seen that the acoustic pressure when L_r = 40 mm, which is the shortest length of the resonator under consideration in the present study, is lower than the corresponding values when L_r = 60 mm and 80 mm, at all the lengths of L_b. As the length of the resonator decreases, the resonance frequency corresponding to the first longitudinal mode increases, which leads to a drop in the amplitude of the acoustic pressure since the resonance frequency and acoustic pressure have an inverse relationship between them. It is also seen that, even though the changes in the acoustic pressure with increasing buffer cylinder length follow different trends when L_r = 60 mm and 80 mm, the highest acoustic pressure is found at L_b = 40 mm in both cases. In contrast to the above, a sharp drop in the acoustic pressure is seen where L_r = 40 mm and L_b = 40 mm. In Fig. 6, the pressure profile along the longitudinal axis of the cell (depicted as X_h in Fig. 1) indicates the presence of wave forms of half the wavelength in both buffer cylinders (X_h = 0 mm to 40 mm and X_h = 80 mm to 120 mm) and in the resonator (X_h = 40 mm to 80 mm). It clearly shows the triggering of the first longitudinal mode of resonance in the resonator and the second longitudinal mode in the buffer cylinders. In fact, the second longitudinal mode does not exist for a single half open cylinder. If a single half open cylinder is combined with a fully opened cylinder as in the H-type cell, however, the second mode should also be excited. It can be inferred, therefore, that the combination of dimensions of the resonator and buffer cylinders, which simultaneously triggers the resonance in both resonator and buffer cylinders, needs to be avoided because the resonance may reduce the amplitude of the photoacoustic response. We believe that this observation should be an important design consideration for the H-type cell.

In the second set, simulations were performed by varying L_b and D_b while the length in the resonator is kept constant at L_r = 40 mm. Fig. 7 shows the acoustic pressure at the location of
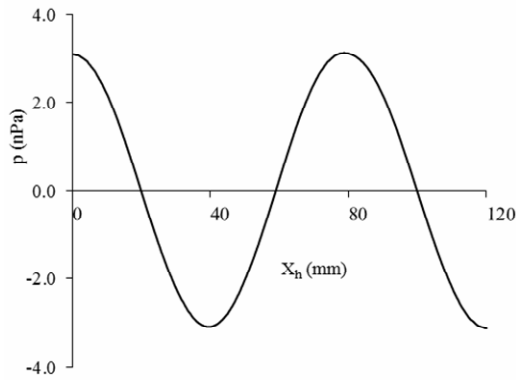
Fig. 6. Variation in the acoustic pressure along the longitudinal axis at $L_b = L_r = 40$ mm for the H-type cell.
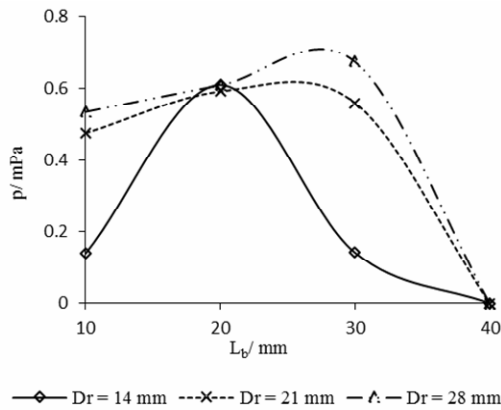
Fig. 7. Variations of the acoustic pressure at the position of microphone with the length of the buffer cylinder at different diameters of the buffer cylinders for the H-type cell. Here, the length of the resonator is kept constant at $L_r = 40$ mm.

microphone plotted against the buffer cylinder length at different diameters of the buffer cylinders. As the diameter of the buffer cylinder increases, the acoustic pressure also increases. This may be due to the fact that, as the buffer cylinder diameter increases, the standing wave gets confined to the resonator, thereby increasing the wave amplitude. When the diameter of the buffer cylinders is small and comparable to that of the resonator, the waveforms, which otherwise would have been confined to the resonator, start propagating to the buffer volumes as well. Coupling of the acoustic fields in the resonator and buffer cylinders distributes the standing wave over both of them, resulting in a lower amplitude of the acoustic pressure. A sharp drop in the acoustic pressure at $L_b = 40$ mm, where the resonance is excited in both resonator and buffer cylinders, is observed in all the cases irrespective of the buffer cylinder diameter.

To understand how the dimensions of the cell affect the energy losses within the cell, the quality factors were calculated for all the simulations mentioned earlier in this section. The quality factors for the simulations shown in Fig. 5 are plotted in Fig. 8. The quality factor decreases with increasing length of the resonator, which is expected because the quality factor
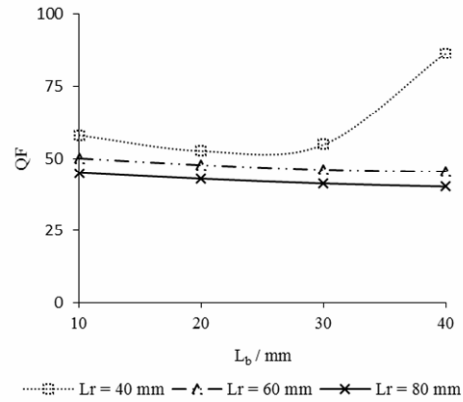
Fig. 8. Variations of the quality factor with the length of the buffer cylinder, at different resonator lengths for the H-type cell. Here, the diameter of the buffer cylinders is kept constant at $D_b = 14$ mm.

is inversely proportional to the square root of the resonator length [3]. The quality factor decreases with increasing buffer cylinder length. As the length increases, the increases in the surface losses dominate the net energy stored in the volume, which results in a lower quality factor. However, a sharp increase in the quality factor for the case where $L_r = 40$ mm and $L_b = 40$ mm is because of the excitation of both resonator and buffer cylinders explained in the previous section, which is not favourable in any case. From the above results, we concluded that a smaller buffer cylinder length is preferred for a high quality factor in the H-type cell.

Even if the first mode of longitudinal resonance frequency corresponding to the resonator length selected is above 1 kHz, the resonance frequency of the cell may vary according to the dimensions of the buffer cylinders. To understand the geometrical effects of the buffer cylinders on the resonance frequency of the cell, the resonance frequency of the first longitudinal mode is plotted against the buffer cylinder length for various simulations, where the resonator length is kept constant at 40 mm as shown in Fig. 9. The resonance frequency varies considerably with the buffer cylinder length. However, the variation in the resonance frequency is minimal if the cylinder length is between 20 mm and 30 mm, implying that the diameter of the buffer cylinders has little effect on the resonance frequency within this range. Similar observation was reported by Cai et al. [7].

3.3 Optimization of the H-type cell

Based on the results from the statistical analysis and parametric study described above, it is evident that, for the H-type cell, a prudent selection of the geometrical parameter is critical to maximize the photoacoustic response within the acceptable limit of resonance frequency. Since numerical simulations on all the combinations of dimensions within the domain of interest may not be possible, a functional relationship between the acoustic pressure at the position of microphone and the geometrical parameters has to be developed. In RSM, the
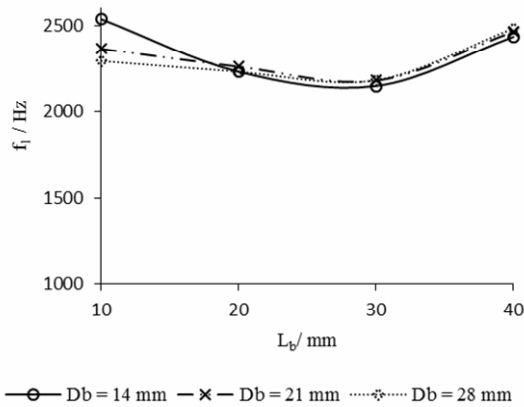
Fig. 9. Variations of the resonance frequency with the length of the buffer cylinders at different diameters of the buffer cylinders, D_b = 14 mm, 21 mm and 28 mm.

response data has to be expressed as a function of independent control parameters, which can be plotted as a surface. As discussed in Subsec. 3.1, though our DOE analysis shows that all four control parameters considered are significant in determining the acoustic pressure, there is a practical constraint in minimizing the diameter of the resonator. So, the other three geometrical dimensions are to be optimized while keeping D_r constant at 6 mm in order to maximize the acoustic pressure, which would be the highest point in the response surface.

In general, a second degree polynomial is widely used for modelling the response in terms of the control variables in a matrix form as follows [20]:

$$y = \beta_0 + \sum_{i=1}^{m} \beta_i x_i + \sum_{i=1}^{m-1} \sum_{j=i+1}^{m} \beta_{ij} x_i x_j + \sum_{i=1}^{m} \beta_{ii} x_i^2 + \varepsilon \quad (14)$$

where y and x_i are the response and control variables respectively, m is the number of control variables, β_i and β_{ij} are the regression coefficients to be determined, and ε is the error between the modelled and actual responses.

Because of the nonlinear nature of the relationship between the acoustic response and control parameters, it is impossible to develop a single functional relationship between a wide domain of values of the control parameters and the corresponding responses. In this study, a 3-D space created by the three control parameters, whose upper and lower limits are selected based on practical considerations, forms the domain of interest. The responses corresponding to various sample points in the domain, which are the combinations of different levels of the control parameters, have to be calculated. The number of sample points should be reasonably chosen so that a meaningful relationship between the response and control parameters can be established with a minimum number of simulations. In order to generate the sample points at which numerical simulations have to be executed, we selected a scheme of central composite design (CCD) [20] which is commonly used in real applications. The domain in the CCD is a cubical space extending to two axial points outside the cube for each axis. The sample points in the CCD are composed of eight corner points, six axial points and one center point. The corner points take care of the first order nature of the response, whereas the axial points, placed away at a distance q from the center, account for the second order relationship between the response and control parameters. Here, the distance is given by $q = Z^{0.25}$, where Z is the number of the corner points. Since $Z = 8$ is used in this study, therefore, five different levels, 0, 1, -1, 1.682 and -1.682 were assigned to each parameter, corresponding to the center, corner and axial points, respectively. The center and corner points of each control parameter should be chosen based on the actual domain of interest after considering the necessary practical constraints. From the initial experiments conducted in Subsec. 3.1, the maximum response was found for the combination of L_r = 80 mm, L_b = 20 mm and D_b = 28 mm. So, it would be ideal to fix the center point of the cubical domain around the above set of control parameters. In the case of L_r, the domain of values is constrained by the minimum allowable frequency, which is determined by electrical noises associated with the microphone and the inverse relationship between the frequency and amplitude of the acoustic pressure. So, we chose to keep the minimum frequency corresponding to the first longitudinal mode at which we wish to operate the cell above 1000 Hz, which is a widely accepted lower cut-off. Considering this constraint, the '0' level of the control parameter L_r is selected as 80 mm. Since we limit the sample points to 15, the domain should be short enough so that the functional relationship, which would be developed based on the correlation between the control parameters and response at the sample points, is realistic.

To minimize the domain, in this study, the corner points are kept at 60 mm and 100 mm. So, the axial points, corresponding to the levels 1.682 and -1.682, are at 113.64 mm and 46.36 mm respectively. In the case of L_b, the center point is at 30 mm and the corner points are at 20 mm and 40 mm. This range of values are chosen based on the theoretical consideration that the buffer length should be approximately a quarter of the wavelength corresponding to the first longitudinal mode. For D_b, since the acoustic pressure is highly sensitive to it, a wider domain of values cannot be represented by our model, which is built on the data from 15 sample points. So, its center is fixed at 28 mm, with the corners at 26 mm and 30 mm. The range of values of D_b considered here is between 4 to 5 times that of D_r, which would minimize the coupling of acoustic waves in the resonator and buffer cylinders, without making the buffer cylinders unnecessarily bulky. For a real life application, this study can be extended to a wider domain of control parameters, which would in turns need the evaluation of response at more number of sample points using numerical simulations. However, since the objective of the present study is only to explore the feasibility of application of the RSM in sizing the cell for the optimal acoustic response, the miniature model to be discussed here would suffice for a demonstrative purpose. The acoustic pressures, measured as responses, are listed in Table 6 according to the design matrix made using CCD.

Table 6. Acoustic pressures at the position of microphone obtained from the numerical simulations at the sample points generated using CCD for the H-type cell.

Trial number	L_r / mm	L_b / mm	D_b / mm	Acoustic pressure / mPa
1	80	30	28	6.986×10^{-1}
2	60	20	26	5.336×10^{-1}
3	100	20	26	5.532×10^{-1}
4	60	40	26	6.018×10^{-1}
5	100	40	26	5.988×10^{-1}
6	60	20	30	6.514×10^{-1}
7	100	20	30	6.986×10^{-1}
8	60	40	30	6.950×10^{-1}
9	100	40	30	6.870×10^{-1}
10	80	13.18	28	6.110×10^{-1}
11	80	46.82	28	6.534×10^{-1}
12	113.64	30	28	6.040×10^{-1}
13	46.36	30	28	6.290×10^{-1}
14	80	30	31.364	5.797×10^{-1}
15	80	30	24.636	4.335×10^{-1}

By using the least square method, all the regression coefficients of the second order polynomial suggested in Eq. (14) were determined based on the data listed in Table 6. The regression model obtained is as follows:

$$p = \begin{pmatrix} -0.000412213 L_r^2 - 0.001095853 L_b^2 \\ -0.138327306 D_b^2 \\ -0.000386438 L_r L_b + 0.000208437 L_r D_b \\ -0.004121875 L_b D_b + 0.07163597 L_r \\ +0.229140165 L_b \\ +8.100274126 D_b - 116.5209411 \end{pmatrix}. \quad (15)$$

The coefficient of determination, R^2, was 0.89 between the modelled and calculated acoustic pressure data. Since there is a nonlinear dependency of the response on the control parameters, which is clearly seen in Figs. 5 and 7, it is hard to obtain a higher coefficient of determination. Using the above equation, an RSM model was developed, which is valid within the cubical space of the chosen levels of the CCD. In this optimization problem, the objective is to maximize the acoustic pressure while maintaining a lower cut off frequency of 1000 Hz for the first longitudinal mode and as mentioned in the Subsec. 3.1, the diameter of the resonator is already fixed at 6 mm.

The result obtained by the RSM model was confirmed by performing a simulation at the optimum setting. The optimal dimensions of the cell and the deviation in the values of acoustic pressure predicted by the model and from the simulation are summarized in Table 7. The variation of acoustic pressure calculated by the optimization model on either side of the optimal value of L_r, while keeping the values of L_b and D_b

Table 7. Optimal dimensions of the H-type cell predicted by the RSM model and the comparison of acoustic pressure between the RSM model and numerical simulation at the optimal setting.

L_r/ mm	L_b/ mm	D_b/ mm	Acoustic pressure predicted by the RSM model / mPa	Acoustic pressure from the simulation / mPa	Deviation / %
76.9	36.8	28.8	7.0517×10^{-1}	7.1471×10^{-1}	1.33
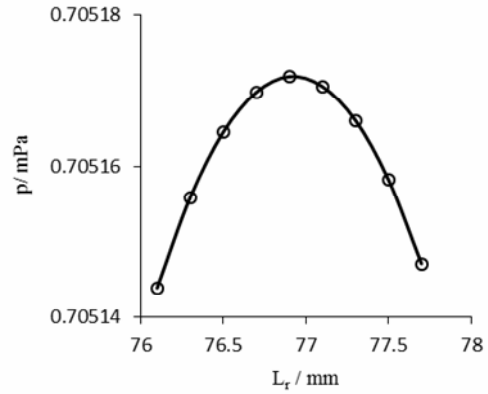
Fig. 10. Variation of the acoustic pressure with the length of resonator cylinder on either side of the optimum length found from the RSM model. Here, the other parameters are kept at the optimal settings suggested by the RSM model.

at the optimal setting, is shown in Fig. 10. Similar plots for L_b and D_b are also shown in Figs. 11 and 12, respectively. All the above three plots confirm the peaking of acoustic pressure at the optimal settings. The deviation between the model and simulation at the optimal setting was found to be within the acceptable range. Hence, the optimal setting of dimensions found by the RSM model can be used for designing the photoacoustic cell with the best sensitivity for the problem considered in the present study. It also shows that the RSM model can be successfully implemented for the optimal dimensions of the H-type cell.

4. Conclusion

In this study, we calculated the photoacoustic response in a resonant photoacoustic cell using linearized forms of the continuity equation, Navier-stokes equation, energy equation and equation of state. The above method, which has already been reported in literature as an effective way of solving various acoustic problems, is also found to be useful enough to build a physically realistic metamodel for dimensional optimization of an H-type resonant photoacoustic cell. We discovered that the simultaneous excitation of resonance in both resonator and buffer cylinders results in a lower acoustic pressure at the position of microphone, which is unfavorable for spectroscopic applications. In order to avoid it, the length of the buffer cylinders should be selected in such a way that the resonance frequency corresponding to any of the modes is not equal to the first longitudinal frequency of the resonator. The effects of the geometrical parameters on the resonance fre-
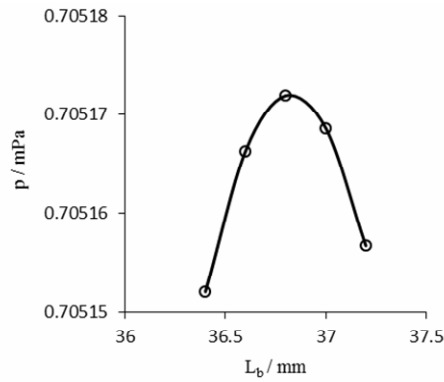
Fig. 11. Variation of the acoustic pressure with the length of buffer cylinder on either side of the optimum length found from the RSM model. Here, the other parameters are kept at the optimal settings suggested by the RSM model.
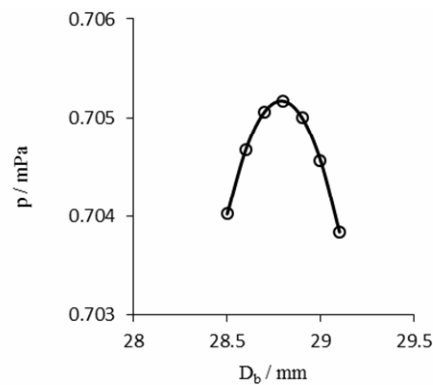
Fig. 12. Variation of the acoustic pressure with the diameter of the buffer cylinder on either side of the optimum diameter found from the RSM model. Here, the other parameters are kept at the optimal settings suggested by the RSM model.

quency and quality factor for the H-type cell have been analyzed. This study also shows that the optimization of dimensions of the H-type cell can be done by applying the response surface methodology. The optimization based on a metamodel would be beneficial in the design and analysis of resonant photoacoustic cells. The optimized model developed in the present study, however, does not take the window noise into consideration. An experimental investigation on the same is necessary to ensure the effectiveness of the optimized cell for practical applications. Apart from that, considering the nonlinear relationship between the geometrical parameters and photoacoustic response, development of a more sophisticated surrogate model such as Kriging technique would be useful, which could be an interesting topic for the future research.

Acknowledgments

Nomenclature

a	: Absorption coefficient of the medium
C_p	: Specific heat at constant pressure
C	: Speed of sound in the medium
D_b	: Diameter of the buffer cylinder
D_r	: Diameter of the resonator
F_X	: F ratio of a control parameter 'X'
f	: Pulsation frequency of the laser
f_j	: Resonance frequency corresponding to mode 'j'
$f_{1,anal}$	: Resonance frequency corresponding to first longitudinal mode obtained from the analytical expression
H'	: Heat addition by laser source
$\boldsymbol{I}$	: Identity matrix
I_0	: Power of the laser
i	: Imaginary unit
j	: Mode of the resonance
k	: Thermal conductivity
L_b	: Length of the buffer cylinder
L_r	: Length of the resonator
N	: Number of experiments
p	: Pressure
q	: Distance of axial points from the center in CCD
Q_j	: Quality factor corresponding to mode 'j'
r	: Radial coordinate of the H- type cell
SS_T	: Total sum of squares
SS_X	: Sum of squares corresponding to a particular parameter 'X'
SS_e	: Sum of squares due to error
t	: Time
T	: Temperature
$\boldsymbol{u}$	: Velocity
y_i	: Response value for a trial
V_e	: Variance of error
V_X	: Variance of a control parameter 'X'
w	: Radius of the laser beam
X_h	: Longitudinal axis of H-type cell
Z	: Number of corner points in CCD
Δf_j	: Full width half maximum (FWHM) at mode 'j'
α	: Thermal expansion coefficient
β_T	: Isothermal compressibility
β_i, β_{ij}	: Regression coefficients
μ	: Dynamic viscosity
μ_B	: Bulk viscosity
ρ	: Density
ϕ_T	: Total degrees of freedom

ϕ_X : Degrees of freedom corresponding to parameter 'X'
ω : Angular frequency of the laser
0 : Equilibrium steady values
'(prime) : Small fluctuation representing the acoustic part of variables

References

[1] A. G. Bell, On the production and reproduction of sound by light, *American Journal of Science*, 20 (118) (1880) 305-324.

[2] A. G. Bell, The production of sound by radiant energy, *Science*, 2 (49) (1881) 242-253.

[3] F. G. C. Bijnen, J. Reuss and F. J. M. Harren, Geometrical optimization of a longitudinal resonant photoacoustic cell for sensitive and fast trace gas detection, *Review of Scientific Instruments*, 67 (8) (1996) 2914-2923.

[4] A. Miklos, P. Hess and Z. Bozoki, Application of acoustic resonators in photoacoustic trace gas analysis and metrology, *Review of Scientific Instruments*, 72 (4) (2001) 1937-1955.

[5] K. A. Gillis, D. K. Havey and J. T. Hodges, Standard photoacoustics spectrometer: Model and validation using O_2 A-band spectra, *Review of Scientific Instruments*, 81 (2010) 064902.

[6] S. Bernegger and M. W. Sigrist, Longitudinal resonant spectrophone for CO-Laser photoacoustic spectroscopy, *Applied Physics B*, 44 (2) (1987) 125-132.

[7] Y. Cai, N. Arsad, M. Li and Y. Wang, Buffer structure optimization of the photoacoustic cell for trace gas detection, *Optoelectronics Letters*, 9 (3) (2013) 233-237.

[8] Y. H. Pao, *Opto acoustic spectroscopy and detection*, Academic, New York (1977).

[9] B. Baumann, B. Kost, H. Groninga and M. Wolff, Eigenmode analysis of photoacoustic sensors via finite element method, *Review of Scientific Instruments*, 77 (2006) 044901.

[10] B. Kost, B. Baumann, M. Germer, M. Wolff and M. Rosenkranz, Numerical shape optimization of photoacoustic resonators, *Applied Physics B*, 102 (1) (2011) 87-93.

[11] A. L. Ulasevich, A. V. Gorelik, A. A. Kouzmouk and V. S. Starovoitov, A miniaturized prototype of resonant banana-shaped photoacoustic cell for gas sensing, *Infrared Physics & Technology*, 60 (2013) 174-182.

[12] P. M. Morse and K. U. Ingard, *Theoretical acoustics*, McGraw-Hill, New York (1968).

[13] B. Baumann, M. Wolff, B. Kost and H. Groninga, Finite element calculation of photoacoustic signal, *Applied Optics*, 46 (7) (2007) 1120-1125.

[14] B. Parvitte, C. Risser, R. Vallon and V. Zeninari, Quantitative simulation of photoacoustic signals using finite element modelling software, *Applied Physics B*, 111 (3) (2013) 383-389.

[15] W. M. Beltman, P. J. M. van der Hoogt, R. M. E. J. Spiering and H. Tijdeman, Implementation and experimental validation of a new viscothermal acoustic finite element for acousto-elastic Problems, *Journal of Sound and Vibration*, 216 (1) (1998) 159-185.

[16] A. Gliere, J. Rouxel, B. Parvitte, S. Boutami and V. Zeninari, A coupled model for the simulation of miniaturized and integrated photoacoustic gas detector, *International Journal of Thermophysics*, 34 (11) (2013) 2119-2135.

[17] L. Duggen, N. Lopes, M. Willatzen and H. G. Rubahn, Finite element simulation of photoacoustic pressure in a resonant photoacoustic cell using lossy boundary conditions, *International Journal of Thermophysics*, 32 (4) (2011) 774-785.

[18] *Acoustic module user's guide version 4.3*, http://www.comsol.com, Accessed on November (2015).

[19] P. J. Ross, *Taguchi techniques for quality engineering*, McGraw-Hill, New York (1988).

[20] A. I. Khuri and S. Mukhopadhyay, Response surface methodology, *WIREs Computational Statistics*, 2 (2010) 128-149.

Madhusoodanan Mannoor received his B.Tech. and M.Tech. degrees from Kerala University and National Institute of Technology, Calicut, India in 2004 and 2007, respectively. Then he worked for four years as a field engineer in Nuclear Power Corporation of India Limited and subsequently as an Assistant Professor in the Department of Mechanical Engineering, at Government Engineering College, Kannur, India. Presently, he is pursuing doctoral studies in the Department of Mechanical Engineering at Dong-A university, Busan, Republic of Korea. His research interests are in the field of photoacoustics, computational fluid dynamics and molecular dynamics.

Jeeseong Hwang received his Ph.D. in condensed matter physics from Michigan State University. Presently he is a research biophysicist in the physical measurement laboratory at the National Institute of Standards and Technology (NIST). Before joining NIST, he was a research scientist in an immunology laboratory at the Biology Department of the Johns Hopkins University. His research in the molecular and biophotonics project focuses on optics and nanobiophotonics for optical medical imaging and quantitative biophysics.

Sangmo Kang received his B.S. and M.S. degrees from Seoul National University, Seoul, Republic of Korea in 1981 and 1987, respectively, and then worked for five years in Daewoo Heavy Industries, Incheon, Republic of Korea as a field engineer. He obtained his Ph.D. in Mechanical Engineering from the University of Michigan, Ann Arbor, USA in 1996. Dr. Kang is currently a Professor in the Department of Mechanical Engineering at Dong-A University, Busan, Republic of Korea. His research interests are in the area of micro and nanofluidics, turbulent flow and photoacoustics combined with the computational fluid dynamics.